Fire spread from MODIS burned area data: obtaining fire dynamics information for every single fire

David Frantz[a,*], Marion Stellmes[a], Achim Röder[a] and Joachim Hill[a]

[a] Environmental Remote Sensing & Geoinformatics, Faculty of Spatial and Environmental Sciences, Trier University, Campus II, Behringstr. 21, 54296 Trier, Germany

* corresponding author: David Frantz, e-Mail: frantz@uni-trier.de

Additional keywords: Fire regime, fire spread, fire dynamics, ignition point, MODIS, single fire

Running head: Fire dynamics from MODIS burned area

Abstract

Fire spread information on a large scale is still a missing key layer for a complete description of fire regimes. We developed a novel multi-level object-based methodology that extracts valuable information about fire dynamics from Moderate Resolution Imaging Spectroradiometer (MODIS) burned area data. Besides the large area capabilities, this approach also derives very detailed information for every single fire regarding timing and location of its ignition, as well as detailed directional multi-temporal spread information. The approach is a top-down approach and a multi-level segmentation strategy is used to gradually refine the individual object-membership. The multi-temporal segmentation alternates between recursive seed point identification and queue-based fire tracking. The algorithm relies on only a few input parameters that control the segmentation with spatial and temporal distance thresholds. We present exemplary results that indicate the potential for further usage of the derived parameters.

Brief summary for the non-specialist reader

A new strategy to derive detailed fire spread information from satellite imagery across large areas is proposed. Single fires are identified and described with respect to the timing and location of their ignition. The daily directional spread information of the fire events is also recorded during this process.

Introduction

The assessment and evaluation of fire-prone ecosystems need a full understanding of the status, variability and change of land cover and land use systems (Stellmes *et al.* 2013). Wildfires are an important component in African landscape ecology for millennia (Clark and Bakker 1964) and are even vital for the maintenance, distribution and function of the savanna state (Bond and Keeley 2005; Staver *et al.* 2011). Therefore, it is of major importance to understand and describe all components of the prevailing fire regime (Van Langevelde *et al.* 2003), including the short-term fire behavior as well as the long term fire dynamics (Li 2000). Important long-term parameters include the fire type, frequency, seasonality, and intensity whereby fire intensity is largely determined by fuel load, its heat yield and fire spread (le Roux 2011). Areal information about the frequency, seasonality, and intensity can be readily obtained from standard fire products (Stellmes *et al.* 2013). The fuel load can be obtained from biomass predictions (Lu 2006) and reasonable heat yield values can be approximated from literature; e.g. Trollope et al. (2004) tabulated values for African grass fuels. Whilst the short-term fire behavior is well understood for single mega fires (Cruz *et al.* 2012), detailed information for all fire events on the regional scale is scarce and not sufficiently explored. Region-wide information about fire behavior, such as per-fire spread rate and propagation direction, fire size, fire duration, and ignition source as well as areal aggregation into fire size distribution or ignition density, will allow for a deeper understanding of different fire regimes and ecological processes. Fire spread is dependent on a large variety of factors, including fuel arrangement (e.g. vertical structure and horizontal continuity), fuel condition (e.g. moisture, aeration, and compaction), fuel type (e.g. grass or canopy), fuel load, topography and local weather (le Roux 2011; Trollope *et al.* 2004), and as such, the complex interaction between fire spread and its determinants can be explored in more detail for large areas. Detailed information of fire sizes and pattern will allow for a more comprehensive assessment of ecological effects (Turner *et al.* 1997), and exploring ignition points and density can provide valuable insight about the anthropogenic influence on human-driven fire regimes (Archibald *et al.* 2009). Assimilating fire size distribution, as e.g. derived by Hantson *et al.* (2015) and fire propagation measurements into dynamic vegetation models improve simulations of global carbon fluxes (Kantzas *et al.* 2015). Similarly, learned knowledge will also be beneficial for the enhancement, calibration and validation of fire propagation simulations, e.g. ignition points may serve as more realistic seeds for the propagation, which in combination with fire risk simulation assessments might support adjusted fire management strategies (Finney 2004; Mbow *et al.* 2004). Up to now, no readily available standard product about continuous fire spread exists, although algorithms like the flooding approach of Archibald and Roy (2009) already approached parts of the problem by deriving individual fire sizes.

Loboda and Csiszar (2007) developed a fire spread reconstruction approach for boreal forests though their usage of active fire input data somewhat limits the widespread applicability. The Moderate Resolution Imaging Spectroradiometer (MODIS) Active Fire product (Giglio *et al.* 2003) can be regarded as a spatially fragmented, snapshot-like data product that has limitations on providing the continuously burned area (Pereira 2003), needed for precise per-fire size estimations and improved object separability (as spatially disconnected fire fronts can either be two separately ignited fires or one progressing fire). On the contrary, the MODIS Burned Area product (Roy *et al.* 2005b; Roy *et al.* 2002) is specifically tailored for providing the continuous areal burned extent.

As such, we propose a novel multi-level object-based methodology that extracts valuable information about fire dynamics over large areas from burned area data. Besides the large area capabilities, this approach also derives very detailed information for every single fire regarding timing and location of its ignition and detailed directional multi-temporal spread information.

Data and study area

We use MODIS Burned Area data (Roy *et al.* 2005b; Roy *et al.* 2002) as input to our algorithm. The burned area product (MCD45A1) gives information about the areal extent and the approximate day of burning of each pixel at 500 m spatial resolution. It is a frequently used global data product that is updated on a regular basis, and as such it was chosen as input data source. However, other similar data sources may also be used as input to our proposed methodology. The smallest reliably detectable burned areas are approximately 1 km^2

(Roy *et al.* 2005a). Burned areas are derived by applying a bi-directional reflectance function (BRDF) model-based change detection algorithm (Roy *et al.* 2002), resulting in a nominal daily temporal resolution. The 'approximate' day of burning is inferred with a nominal uncertainty of fewer than 8 days (Roy *et al.* 2005b), and the observed precision compared to active fire detections is better in most parts of the world (Boschetti *et al.* 2010): 50% and 75% of the detections are detected within 1 day and within 4 days, respectively. The precision is worse in areas with persistent cloud coverage at MODIS overpass time; e.g. in South-East Asia, only 75% of the detections are within the nominal accuracy of ±8 days. However, the non-perfect temporal accuracy results in some degree of spatio-temporal scatter which was needed to be reflected in the following algorithm design.

The monthly burn date information is extracted from the hierarchical data format (HDF), and an image stack for the complete time series is compiled. Several MODIS tiles may be mosaicked to one single input file. The data need to be projected to a locally adapted coordinate system, as the generic MODIS sinusoidal projection is non-conformal. However, it needs to be stated that the requirement of conformality and equality of area cannot be satisfied with a single projection, and thus, small inaccuracies in either the directional or areal estimates are unavoidable. For our Southern African study area, we chose a Lambert Azimuthal Equal Area projection, centered in the middle of the study area at 18°S / 26°E. The reported fire sizes will be accurate, and the directional spread information might be distorted to a small degree as scale decreases radially as the distance increases from the center (Snyder 1987). The maximum directional distortion is 7.5° in azimuth, and for the majority of the study area it is well below this value; given that we gather directional information in coarse 45° intervals, we consider this acceptable.

We developed the method in continental sub-equatorial Africa, as being one of the most fire-prone regions in the world (Dwyer *et al.* 2000) with little information about the spatial and temporal fire size distribution (Roy *et al.* 2005a). The study area ranges from the tropics to South Africa, where fires primarily occur in the savanna ecosystems (Scholes *et al.* 1996), due to a fire feedback mechanism that led to alternative stable states of forest and savanna. Frequent burning suppresses recruitment of saplings to trees, while tree cover suppresses the amount of flammable grass fuel (Staver *et al.* 2011). The continental fire season coincides with the cloud-free dry season lasting from May to October (Scholes *et al.* 1996). However, the area is also home to a variety of different fire regimes, characterized by differences in the overall burned area, fire seasonality, frequency, and intensity (Stellmes *et al.* 2013). Therefore, the study area is an ideal testbed for fire-related algorithm development.

Fire definition

For the purpose of algorithm design, we formally define “fire” in the following. Fire is characterized by spatially continuous fuel consumption along an active fire front in any direction (head fire, back fire or flank fire), i.e. burned areas need to be spatially connected. The fire front is assumed to be active for a limited temporal window, and a fire might continue after a short smouldering / resting period within this window. Any ignition starts an individual fire; this also applies to secondary ignition due to spotting. As a compromise between real-world behavior and algorithmic considerations, individual fires remain separate after coalescence, and the fire propagation thereafter is partitioned into the original fires in order to generate a reasonable fire size distribution. Each fire contains exactly one ignition point.

Methods

We developed an approach that identifies the fire ignition points and tracks the growth of every single fire in MODIS burned area data. Highly valuable information about fire dynamics is recorded during this process. The workflow of the approach is outlined in Fig. 1 with references to the sections and sub-sections. The approach relies on a few tweakable input parameters that are summarized in table 1. The presented results were obtained with the default parametrization.

Please place Table 1 approximately here (column-wide).

Please place Fig. 1 approximately here (column-wide).

Derivation of the fire season

Our algorithm processes each burning season individually, although the complete time series of the monthly burn dates is input at once; the seasons are processed in parallel using the OpenMP API. A main assumption is that a fire season lasts for one year and that there is only one fire per season and pixel. We are aware that this is not always the case but previously presented datasets for Southern Africa (Stellmes *et al.* 2013) indicated that multiple burns are rare, e.g. less than 0.59‰ of all burned pixels in the 2010 burning season. The start of the burning season is derived from the data and is defined as the month with minimum burning activity; in our study area the seasons start in January. Therefore, a single-layer input is compiled from the first recorded fire for each pixel (x,y) in a given season; see Fig. 2 (*a*) for an example. The burn date is encoded as the Day-of-Season (DOS) the land surface burned, i.e. days are measured relative to the start of the burning season. To lessen the impact of temporal detection inaccuracy in the MODIS burned area product, the seasonal input layers are smoothed using a spatially-adaptive lowpass filter with kernel radius D_l.

Step one: fire tracking

The basic idea is to identify the fire ignition points (ch. 1) and to track the growing fires (ch. 2) while proceeding continuously through time. New ignition seeds may be generated at each time step (ch. 3).

Assuming that fires do not leap over larger distances, we segment the input fire layer in order to generate connected patches. These are referred to as Level-0 (L0) objects; see Fig. 2 (*b*) for an example. Each L0-object may contain several individual fires which are attempted to be separated in the next steps. As such, our approach can be considered a multi-temporal top-down approach where a multi-level segmentation strategy is employed to gradually refine the individual object-membership. Optionally, L0-objects that are smaller than n_{min} pixels may be deleted; n_{min} is a tweakable input parameter that allows the rigorous rejection of small and isolated fires (which might be false positive detections). If n_{min} is set to 0, all patches pass.

1) Seed clump identification

All pixels that were burned at DOS $d = 1$ are identified as fire seed point. As a consequence of the MODIS burned area processing strategy (Roy *et al.* 2002), the MCD45A1 product only provides the 'approximate' day of burning. As such, there are several seed points that actually belong to the same fire but are scattered and do not form one connected patch. This spatio-temporal noise necessitates a relatively complex rule-set of pixel-to-object membership. As such, the seed points s_{xy} (with k being the number of seed pixels) are merged into seed clumps using a recursive approach; see Fig. 2 (*c*) for an example. We start with the first potential seed point $s_{xy,0}$ and test if there is any $s_{xy,k}$ around it - within the seed search distance D_s. As a further constraint, $s_{xy,k}$ must also be a member of the same L0-object - if not, the seeds remain separate, i.e. two seed clumps. If a match is found, the procedure is recursively repeated until there is no matching $s_{xy,k}$ left. All $s_{xy,k}$ are then added to a new segmentation layer (Level 1) and are labeled with a unique patch identifier (ID) for each seed clump. This procedure is repeated until each $s_{xy,k}$ was transferred to the L1-segmentation, which holds the seed points of all L1-objects (starting at $d = 1$) with an ascending and unique patch ID. In addition, we record the centroid c_{xy} of the seed clumps ($\triangleq$ ignition point) in an associated array. In the case, that an ignition point is not within its L0-object, c_{xy} is moved using a spiral search, i.e. it is snapped to the L0-object. In the following, fires may propagate from each seed point within a seed clump.

2) Object tracking

We proceed stepwise trough time with $d = [2,366]$ and track the growth of each previously generated L1-object with a queue strategy. Only pixels that (i) are at the edge of L1-objects ($\triangleq$ fire front) and (ii) are temporally close enough to the current d ($\triangleq$ active fire) are considered as potential growing points g_{xy}. The temporal distance is controlled by an input parameter D_t. As such, each g_{xy} is pushed into a first-in-first-out (FIFO) queue. After enqueuing the last g_{xy}, the pixels (g_{xy}) are dequeued one after another and it is tested if there is a newly (time = d) burned pixel b_{xy} within a search radius D_r, which belongs to the same L0-object as g_{xy}. If so, this pixel belongs to the same patch and is labeled accordingly in the L1-segmentation. Afterward, this pixel is also enqueued (g_{xy}) and new pixels b_{xy} in its neighborhood may be appended. This process terminates once the FIFO is completely emptied; see Fig. 2 (*d*) and (*f*) for an example. The FIFO strategy was chosen to avoid a spatial bias as it would be present in a traditional recursive approach. Furthermore, variety in the image looping direction was implemented to prevent a local spatial bias in the case of fire coalescence and to fulfill the theoretical assumption that the fire propagation after coalescence is equally partitioned into the original fires. The looping direction is changed in every iteration as follows: (i) upper-left to lower-right, (ii) lower-right to upper-left, (iii) upper-right to lower-left and (iv) lower-left to upper-right. The same principle is also applied to the looping direction of the local search after dequeuing a burned pixel.

3) Identification of new seed points

All remaining pixels b_{xy} which were burned at time d are assumed to be newly ignited fires (i.e. pixels that were too far away from existing L1-objects or are members of other L0-objects). Thus, new seed-points are obtained by using the previously described method (1) and the new objects are added to the L1-segmentation see Fig. 2 (*e*) for an example. Afterward, d is incremented and the alternating procedure between tracking of fires and adding new fires continues until the end of the season (see Fig. 1).

Please place Fig. 2 approximately here (page-wide).

Step two: re-assignment of non-seed patches

On one hand, the involvement of the search distances enables the tracking of individual fires at all (due to the temporal noise within the MCD45A1 product). On the other hand, the use of the search distances also produces some non-meaningful object assignments if the distribution of the burn dates and/or the patch shapes are unfavorable: multipart L1-objects within the same L0-object might occur. As we do not permit multipart-objects, a second step that enforces the detection of single-part fires was implemented. A real-data example is given in Fig. 7.

We start by sub-segmenting the L1-segmentation (Level-2), such that each L1-multi-object part is assigned a unique patch ID. Each L2-object that does not contain a seed point, is assumed to be invalid and should be either merged with an adjacent L1-object or should become a self-contained L1-object with a new seed point.

1) Re-assignment of invalid sub-patches

Each invalid L2-object is investigated in detail in an iterative procedure. If there is, at least, one neighboring valid L2-object, the invalid patch might be reassigned to the valid one. A reassignment is realized if the mean temporal distance between the boundary pixels is less than $2 \cdot D_t$: the invalid object is labeled accordingly in the L1-segmentation and the L2-object is set to a valid state. In the case of multiple valid neighbors, the temporally closest object is selected. Parts of the boundary may not coincide with the location of fire progression, and as such, D_t was doubled for this purpose. This step is repeated until the number of invalid patches does not change anymore between the iterations.

2) Conversion of invalid sub-patches to new objects

If the latter iteration stopped before all objects are valid, the oldest invalid L2-objects (containing the oldest burn date pixels) are identified, new seed points and new L1-objects are created. The corresponding L2-objects are set to the valid state. Afterward, the re-assignment procedure is resumed (1). This alternating procedure between re-assignments and converting invalid objects proceeds until all patches are eventually valid (see Fig. 1).

Summary of obtained fire dynamics descriptors

The presented method enables the retrieval of several highly valuable fire dynamics descriptors:

As we track and segment every single fire, we obtain information about the total number of fires, individual fire sizes, fire lifetimes, ignition times and locations. In addition, we also gather detailed spread rate information. We not only record the total spread rate (i.e. the growth of the burned area between every time step), we also record directional data: the spread rate is monitored in 8 directions. The directional spread is measured relative to the ignition points. We present the potential of the resulting data in the results section.

Sensitivity analysis and model performance on simulated data

A simulation study was performed to demonstrate the functionality of the approach with respects to the temporally inaccurate input data and to obtain an informed guess about the parameterization. For this purpose, a synthetic input image was generated; see Fig. 3 (*a*). Low DOS values were initialized in the four corners and the DOS values were increased towards the center, simulating four fires emerging from the corners and clashing at horizontal and vertical lines in the center. Noise was added to the simulated data using random numbers for the normal distribution with sigma = 3.5. The noise model overestimates the uncertainty observed in the MODIS data; 50% and 75% of the random numbers alter the values by less than 2.5 days and 4 days, respectively. Only 22% of the random numbers are within 1 day. The fire tracking algorithm was applied to the simulated map using a multitude of parameter combinations (D_s = [2,15], D_r = [2,15], D_t = [1,3,5], D_l = [1,3,5]), and the resulting number of detected fires was visualized in Fig. 4. A bad parameterization results in a very large fire number, e.g. low D_r, whereas several parameterizations resulted in a correct segmentation. The correct fire number (4) is visualized with the black point signature. Although even very high thresholds result in correct segmentations, such a parameterization is not feasible in practice as it would have adverse effects on the delineation of small and densely packed fires. Based on this sensitivity study, which reflects the data uncertainty, and practical tests with the MODIS data, we found following parameterization instrumental: D_s = 10, D_r = 10, D_t = 5 and D_l = 3 (see table 1). If only isolated and large fires exist, larger distances (especially D_t) might be feasible. In areas where the date uncertainty is higher, e.g. in cloud-dominated South-Eastern Asia, higher thresholds for D_t and D_l might be necessary. The resulting segmentation is displayed in Fig. 3 (*b*); the detected ignition points are plotted as point signatures.

A similar simulation was performed to demonstrate the algorithm behavior in the case of fire coalescence; see Fig. 3 (*c*). Low DOS values were initialized in the upper and lower left corners and the DOS values were increased on the diagonals to the center, and from the center to the right margin, thus simulating a fire which progresses after coalescence. Noise was added to the simulation and the fire tracking algorithm was applied. The segmentation is shown in Fig. 3 (*d*); the detected ignition points are plotted as point signatures. The algorithm identified 2 fires and the fire progress after coalescence is shared equally by both fires.

Please place Fig. 3 approximately here (column-wide).

Please place Fig. 4 approximately here (page-wide).

Results and discussion

We applied the fire tracking algorithm to each season of MODIS operation, which in Southern Africa coincides with the calendar years. We parameterized the code with $D_s = 10$, $D_r = 10$, $D_t = 5$, $D_l = 3$ and $n_{min} = 2$ (Table 1). A selected overview of obtained data is shown in Table 2. There are plenty fires in each season and the inter-annual number of fires is quite constant. The results of 2000 and 2001 should be interpreted with care though: Aqua was commissioned in 2001 and as such, the quality of the MCD45A1 product is assumed to be worse till then. In addition, there were no data for June 2001 due to sensor outages, which could explain the lower numbers in 2001. Terra was commissioned in April 2000, therefore, there was no complete coverage for 2000. Nevertheless, the results should not be affected too much by this because the main fire season starts not until June (Stellmes *et al.* 2013). The remaining seasons have full coverage and as such they can be regarded as reliable.

Please place Table 2 approximately here.

Fig. 5 (*a*-*e*) exemplarily displays some of the derived parameters for season 6 in a gridded representation (average values per 1-degree cell). Large differences in the fire regimes are apparent, where e.g. northern Angola is characterized by a large amount of fires (*a*) with relatively low size (*b*) and intermediate duration (*c*). The fire spread rate (*d*) is low to intermediate and the fires are ignited early in the dry season (*e*). Opposed to that, the fire regime in the Angolan / Namibian border region is very different. There are few fires (*a*), but they are large (*b*) and burn fast (*c*), resulting in large spread rates (*d*). Potentially, the late date of ignition (*e*) causes the prevailing grass fuel to be hard-dry, which might result in fast and hot, uncontrollable wildfires. For the majority of the study area, the results are expected to be reliable as the fire season coincides with the nearly cloud-free dry season, whereas there might be a higher inaccuracy in the tropics as persistent cloud coverage decreases the input data quality (Boschetti *et al.* 2010).

Fig. 5 (*f*) is a detailed representation of the data in (*b*) and (*e*) for the subset indicated by the blue box (Angolan / Namibian border region). Each individual fire is visualized, emphasizing the potential to derive per-fire parameters. The point centroids indicate the location the fire was ignited (c_{xy}), the symbol size represents the fire size and the colors indicate the ignition time.

As there are large differences between different fire regime descriptors, we propose to investigate a fire regime and its impact on the environment with a multitude of fire-related parameters due to the complex and partially contradicting information of single parameters.

Please place Fig. 5 approximately here (page-wide).

A subset of the input data (smoothed burn dates) for season 6 and the L1-segmentation (black boundaries) of a large L0-fire is shown in Fig. 6. We visualized the approximate burning trajectories (manually drawn) with arrows that originate in the detected ignition points. The L0-fire was burned between DOS 202 and 292, and affected 5577.25 km^2 of land. Our algorithm was able to track the fire spread and segmented the objects reasonably. There are a number of clashing fires that cease after convergence, e.g. the fire marked by the green ignition point converges both with the blue and upper yellow one. Other fires are affected by coalescence, e.g. the fires marked by the yellow ignition point. They remain separate after coalescence and advance until they run into another fire (upper yellow fire) or cease otherwise (lower yellow fire). The L1-segmentation of a subset (black box) is shown in Fig. 7, before (*a*) and after the re-assignment of invalid patches (*b*). As a consequence of the implemented tracking distance in combination with the FIFO strategy and the temporally inaccurate input data, the L1-segmentation is partly erroneous. This mainly applies to clashing or coalescing objects which are mixed up to a certain degree. The re-assignment step largely corrects for this problem and the resulting L1-objects are better defined after this procedure. Only smaller mixing artifacts remain along the object boundary. The re-assignment step enforces that each L1-object is spatially connected and has one ignition point.

Please place Fig. 6 approximately here (page-wide).

Please place Fig. 7 approximately here (column-wide).

Fig. 8 (*a*) displays the total directional spread of the object marked by the blue ignition point in Fig. 6; the fire mainly moved westward. Fig. 6 clearly supports this. More detailed information on the directional spread of this fire is shown in Fig. 8 (*c*). The stacked spread rates per DOS are shown. The fire advanced in two main pushes to the West and then slowly progressed to North-West. The first push was also accompanied by back and flank fires progressing in all directions, whereas the second push was merely in West direction, accompanied by progression towards North-West and South-West.

Such detailed data exist for every single fire that was delineated with our algorithm. Fig. 8 (*b*) and (*d*) again display the total directional spread and the directional spread rates but cumulated for all fires in season 6. Fig. 8 (*b*) indicates that there is no predominant direction as the directional spread is dependent on a complex set of variables, among them fuel arrangement (e.g. vertical structure and horizontal continuity), fuel condition (e.g. moisture, aeration, and compaction), fuel type (e.g. grass or canopy), fuel load, topography and local weather (le Roux 2011; Trollope *et al.* 2004). This is underpinned by Fig. 6, as different fires advance in entirely different directions. The timing of the fire season is clearly visible in Fig. 8 (*d*) and it is also evident that burning is not continuous, but there are fire waves.

Please place Fig. 8 approximately here (column-wide).

Conclusions and outlook

We developed a multi-level object-based fire-tracking algorithm for use with MCD45A1 data. We were able to extract numerous valuable parameters during the tracking process. The resulting dataset contains very detailed and in part novel information on the movement of fires regarding

- the location and time of the ignition,
- the duration of burning,
- the total size,
- the directional sizes,
- the total daily spread rates and
- the directional spread information.

Such data is inferred for every single fire and paves the way for several future analyses, enabling the derivation of still missing fire regime descriptors at larger scales that provide additional knowledge of fire dynamics. The derived parameters might thus help to improve the discrimination of different fire regimes in a spatially explicit manner and hence, provide new insights about ecological impacts and effects of differing fire management practices (Turner *et al.* 1997), and thus support the development of adjusted fire management strategies (Mbow *et al.* 2004). Vegetation dynamics can be more precisely described and modelled using measured fire size distribution over larger regions (Hantson *et al.* 2015), and can thus improve the accuracy of global carbon simulations (Kantzas *et al.* 2015). The anthropogenic influence of ignition and fire propagation might be better understood (Archibald *et al.* 2009) and fire propagation simulations may be enhanced, calibrated and validated (Finney 2004).

The algorithm is based on only a few tweakable input parameters and can be easily applied. The input parameters control the segmentation, where the spatial and temporal distance thresholds dictate how the multi-scale objects are assembled. We developed the method in Southern Africa, but it can easily be applied to other parts of the world. It would also be possible to input other burned area products – or non-fire data, provided their structure is similar; e.g. multi-temporal clearing or flooding datasets.

Acknowledgment

The MODIS MCD45A1 data product is courtesy of the online Data Pool at the NASA Land Processes Distributed Active Archive Center (LP DAAC), USGS/Earth Resources Observation and Science (EROS) Center, Sioux Falls, South Dakota (https://lpdaac.usgs.gov/data_access). This work was funded by the Federal Ministry of Education and Research under contract number FKZ-01LG1201C as part of the Southern African Science Service Centre for Climate Change and Adaptive Land Management project. We thank the reviewers and editors for their very helpful and constructive comments that significantly improved the quality of the manuscript.

Conflict of Interest

The authors declare no conflict of interest

References

Archibald S, Roy DP, Van Wilgen BW, Scholes RJ (2009) What limits fire? An examination of drivers of burnt area in Southern Africa. *Global Change Biology* **15**(3), 613-630.

Archibald S, Roy DP (2009) Identifying individual fires from satellite-derived burned area data. 2009 IEEE International Geoscience and Remote Sensing Symposium Proceedings, pp. 160-163.

Bond WJ, Keeley JE (2005) Fire as a global 'herbivore': the ecology and evolution of flammable ecosystems. *Trends in Ecology & Evolution* **20**(7), 387-394.

Boschetti L, Roy DP, Justice CO, Giglio L (2010) Global assessment of the temporal reporting accuracy and precision of the MODIS burned area product. *International Journal of Wildland Fire* **19**(6), 705-709.

Clark JD, Bakker EMVZ (1964) Prehistoric Culture and Pleistocene Vegetation at the Kalambo Falls, Northern Rhodesia. *Nature* **201**(4923), 971-975.

Cruz MG, Sullivan AL, Gould JS, Sims NC, Bannister AJ, Hollis JJ, Hurley RJ (2012) Anatomy of a catastrophic wildfire: The Black Saturday Kilmore East fire in Victoria, Australia. *Forest Ecology and Management* **284**(0), 269-285.

Dwyer E, Pinnock S, Gregoire JM, Pereira JMC (2000) Global spatial and temporal distribution of vegetation fire as determined from satellite observations. *International Journal of Remote Sensing* **21**(6-7), 1289-1302.

Finney MA (2004) FARSITE: Fire area simulator: model development and evaluation.

Giglio L, Descloitres J, Justice CO, Kaufman YJ (2003) An Enhanced Contextual Fire Detection Algorithm for MODIS. *Remote Sensing of Environment* **87**(2–3), 273-282.

Hantson S, Pueyo S, Chuvieco E (2015) Global fire size distribution is driven by human impact and climate. *Global Ecology and Biogeography* **24**(1), 77-86.

Kantzas EP, Quegan S, Lomas M (2015) Improving the representation of fire disturbance in dynamic vegetation models by assimilating satellite data: a case study over the Arctic. *Geosci. Model Dev.* **8**(8), 2597-2609.

le Roux J (2011) The effect of land use practices on the spatial and temporal characteristics of savanna fires in Namibia. Ph.D. dissertation Thesis, Friedrich-Alexander-Universität, Erlangen-Nürnberg,

Li C (2000) Fire regimes and their simulation with reference to Ontario. In 'Ecology of a managed terrestrial landscape: patterns and processes of forest landscapes in Ontario.' (Eds AH Perera, DL Euler and ID Thompson) pp. 115-140. (UBC Press: Vancouver, Canada)

Loboda TV, Csiszar IA (2007) Reconstruction of fire spread within wildland fire events in Northern Eurasia from the MODIS active fire product. *Global and Planetary Change* **56**(3–4), 258-273.

Lu D (2006) The potential and challenge of remote sensing-based biomass estimation. *International Journal of Remote Sensing* **27**(7), 1297-1328.

Mbow C, Goïta K, Bénié GB (2004) Spectral indices and fire behavior simulation for fire risk assessment in savanna ecosystems. *Remote Sensing of Environment* **91**(1), 1-13.

Pereira JMC (2003) Remote sensing of burned areas in tropical savannas. *International Journal of Wildland Fire* **12**(4), 259-270.

Roy DP, Frost PGH, *et al*. (2005a) The Southern Africa Fire Network (SAFNet) regional burned-area product-validation protocol. *International Journal of Remote Sensing* **26**(19), 4265-4292.

Roy DP, Jin Y, Lewis PE, Justice CO (2005b) Prototyping a global algorithm for systematic fire-affected area mapping using MODIS time series data. *Remote Sensing of Environment* **97**(2), 137-162.

Roy DP, Lewis PE, Justice CO (2002) Burned area mapping using multi-temporal moderate spatial resolution data—a bi-directional reflectance model-based expectation approach. *Remote Sensing of Environment* **83**(1–2), 263-286.

Scholes R, Kendall J, Justice C (1996) The quantity of biomass burned in southern Africa. *Journal of Geophysical Research: Atmospheres (1984–2012)* **101**(D19), 23667-23676.

Snyder JP (1987) 'Map projections--A working manual.' (USGPO)

Staver AC, Archibald S, Levin S (2011) Tree cover in sub-Saharan Africa: Rainfall and fire constrain forest and savanna as alternative stable states. *Ecology* **92**(5), 1063-1072.

Stellmes M, Frantz D, Finckh M, Revermann R (2013) Fire frequency, fire seasonality and fire intensity within the Okavango region derived from MODIS fire products. In 'Biodiversity & Ecology 5 - Special Volume: Environmental Assessments in the Okavango Region.' (Eds J Oldeland, C Erb, M Finckh and N Jürgens) pp. 351-362. (University of Hamburg)

Trollope WSW, de Ronde C, Geldenhuys CJ (2004) Fire Behaviour. In 'Wildland Fire Management Handbook for Sub-Sahara Africa.' (Eds JG Goldammer and C De Ronde) pp. 199-217. (Global Fire Monitoring Center)

Turner MG, Romme WH, Gardner RH, Hargrove WW (1997) Effects of fire size and pattern on early succession in Yellowstone National Park. *Ecological Monographs* **67**(4), 411-433.

Van Langevelde F, Van De Vijver CADM, *et al*. (2003) Effects of fire and herbivory on the stability of savanna ecosystems. *Ecology* **84**(2), 337-350.

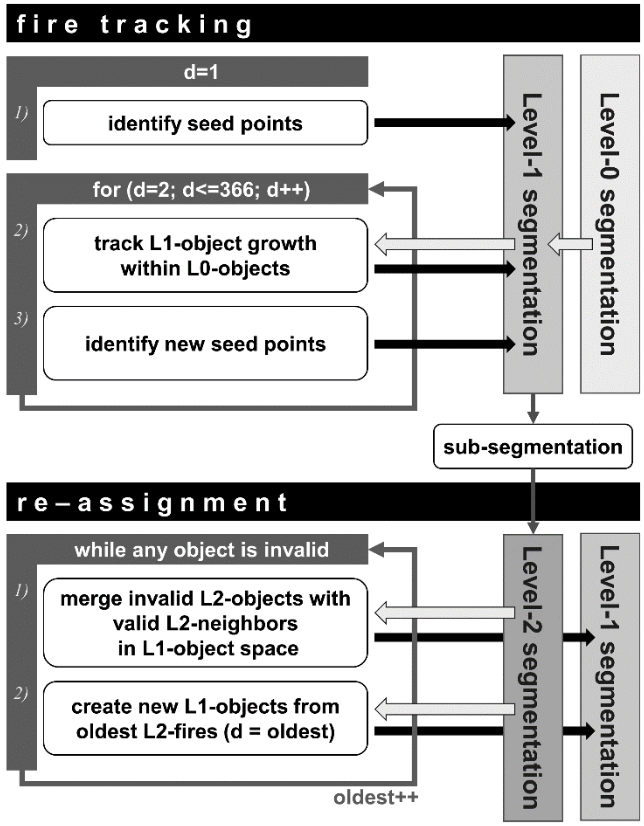

Fig. 1. Workflow of the implemented fire tracking algorithm with references to the sections and sub-sections.

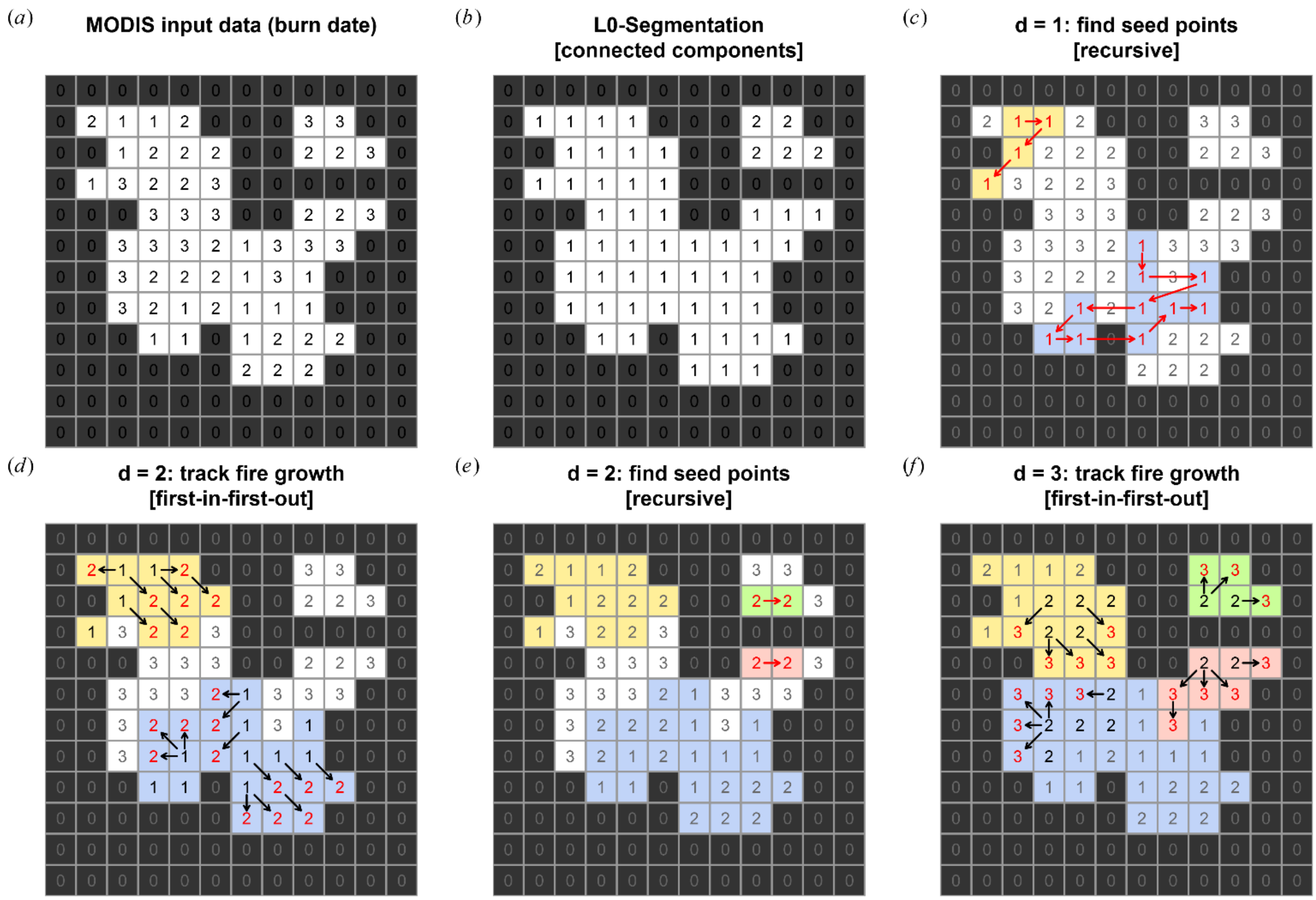

Fig. 2. Step-by-step visualization of the fire tracking algorithm with arbitrary data in a simplified form. The numbers indicate the burning date (DOS) or the L0-segmentation, respectively. Different colors denote different L1-objects. Red numbers indicate pixels that match the current d (DOS) and are selected for seed points s_{xy} or fire growth pixels b_{xy}; black numbers indicate pixels that are potential growing points g_{xy}. Red arrows visualize the recursive seed point aggregation; black arrows visualize the first-in-first-out-based fire growth tracking. For demonstration purposes only, we set $D_s = 2$, $D_r = 1$, $D_t = 1$, $D_l = 0$ and $n_{min} = 2$, as such, complex skipping behavior is not demonstrated. The change of looping direction was also not taken into account for simplicity.

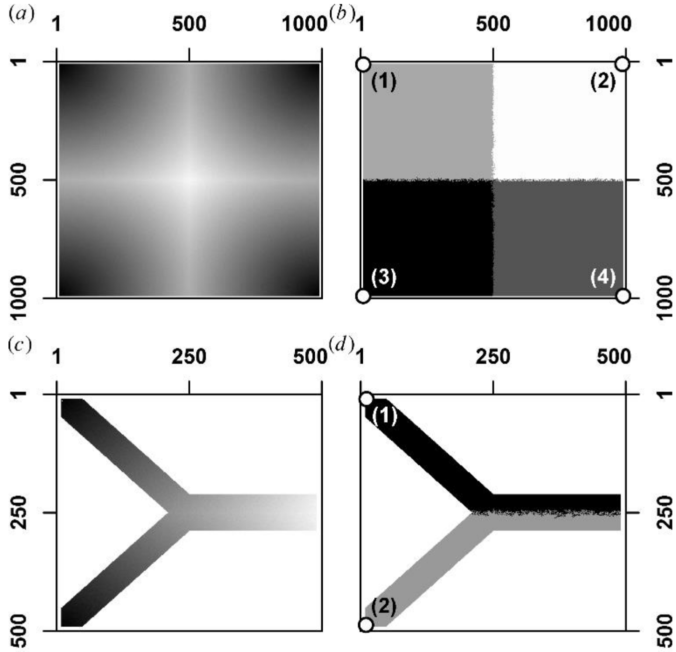

Fig. 3. Simulated burned area maps (*a*,*c*) and resulting segmentation (*b*,*d*). The detected ignition points are superimposed as point signature and the L1-objects are labeled. (*a*–*b*): four clashing fires were simulated. (*c*–*d*): two coalescing fires were simulated.

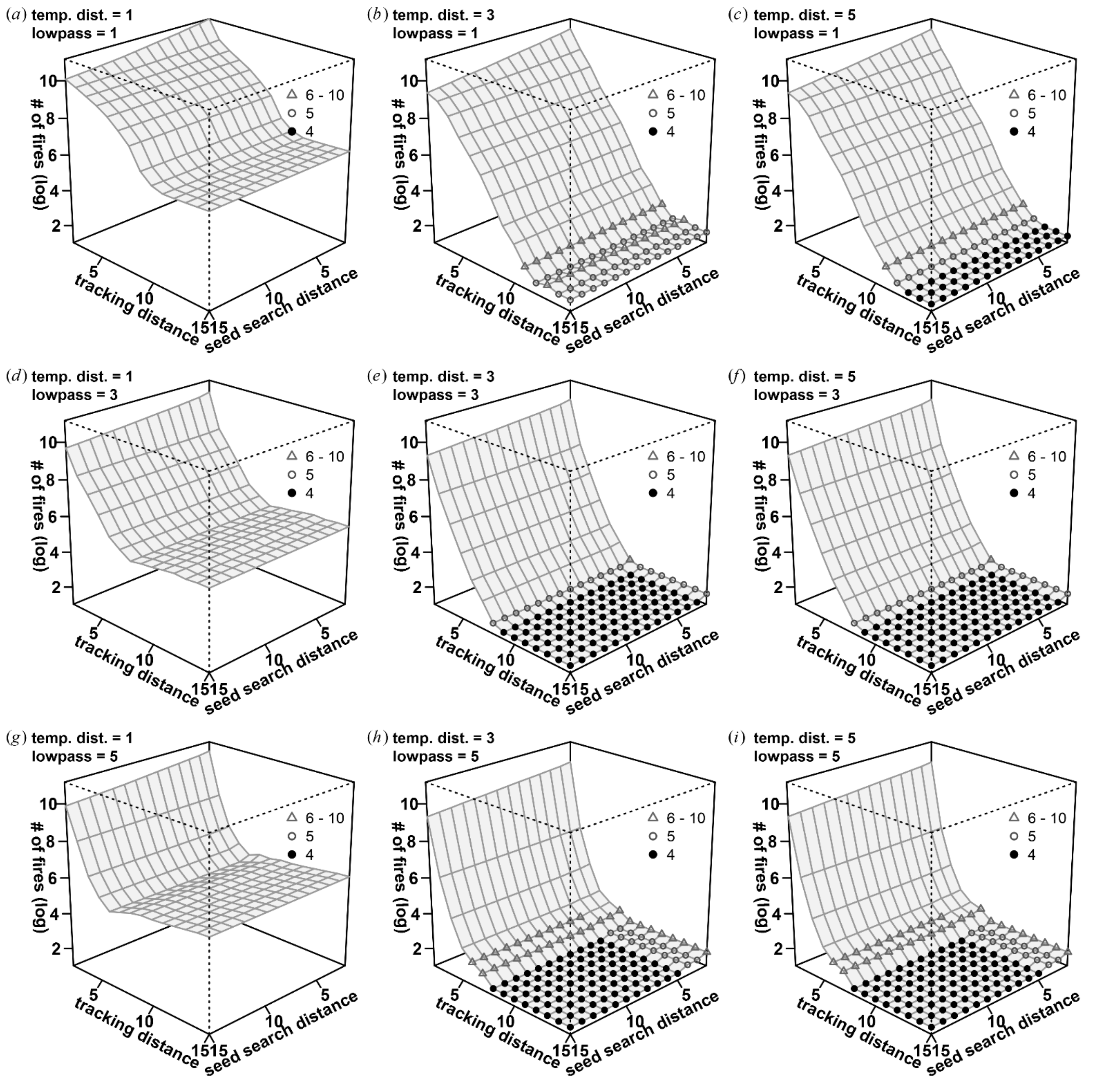

Fig. 4. Sensitivity study for the simulated burned area map in Fig. 3 (*a*), depicting the number of delineated fires. The z-axis is drawn logarithmic; the correct number of fires (4) is plotted as black point signature. The fire tracking algorithm was applied to the simulated map using a multitude of parameter combinations with seed search distance D_s = [2,15], tracking distance D_r = [2,15], temporal distance D_t = [1,3,5], and lowpass kernel size D_l = [1,3,5]. The surfaces are drawn with dependence on D_s and D_r for different D_t and D_l values in (*a*–*i*).

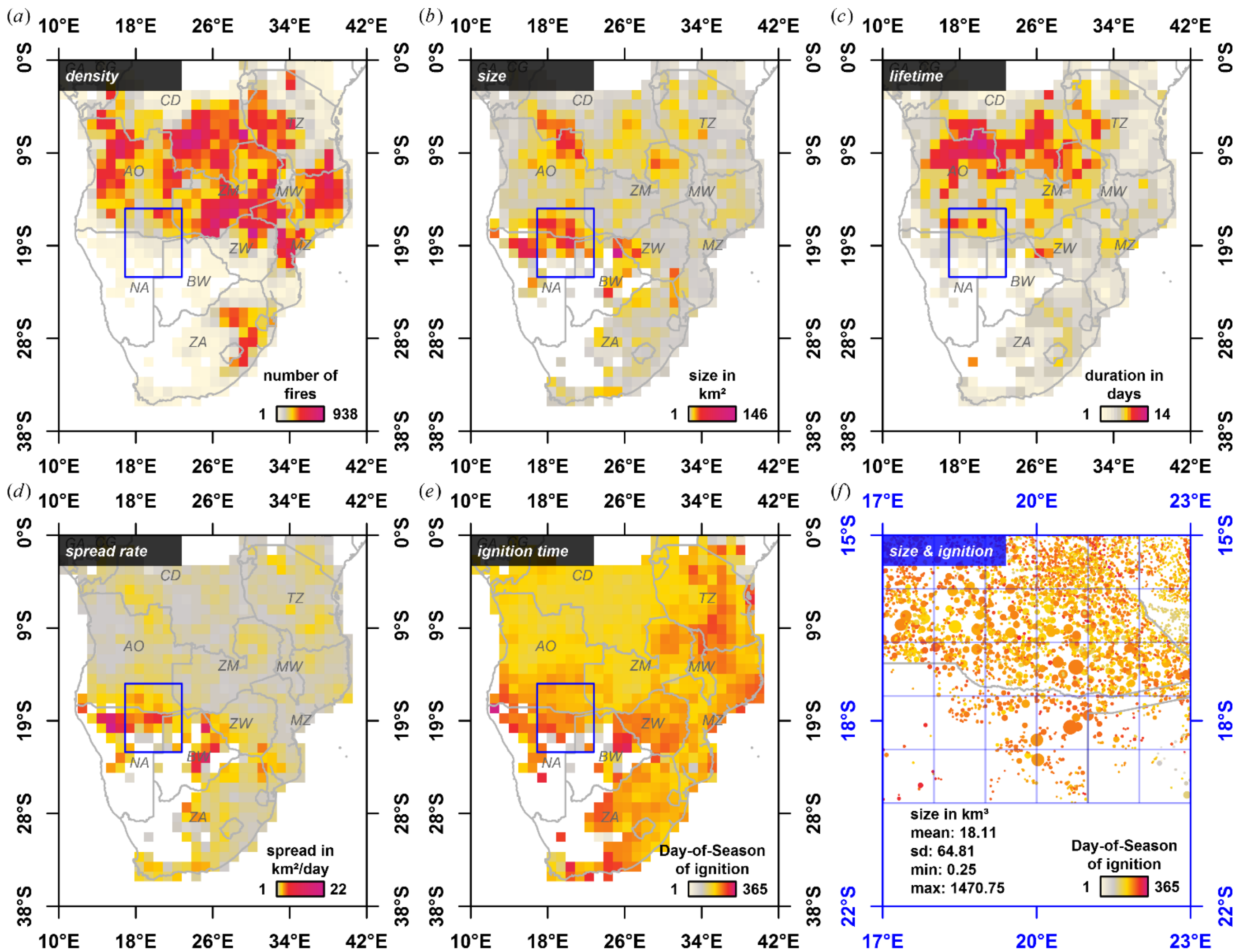

Fig. 5. Spatial visualization of various fire descriptors for fire season 6. (*a*-*e*): Aggregated parameters; 1-degree cells were used for averaging. (*a*): Fire density, i.e. number of fires per grid cell. (*b*): Fire size in km². (*c*): Fire lifetime in days. (*d*): Fire spread rate in km²/day, i.e. fire size / lifetime. (*e*): Ignition date as Day-of-Season. (*f*): Fire size (indicated by symbol size), ignition time (colors) and location of ignition (symbol centroid) for all individual fires in the marked subset, i.e. the blue box in (*a*-*e*); please note that the symbol sizes are drawn with a root-based transfer function. The blue grid matches the 1-degree cells in (*a*–*e*).

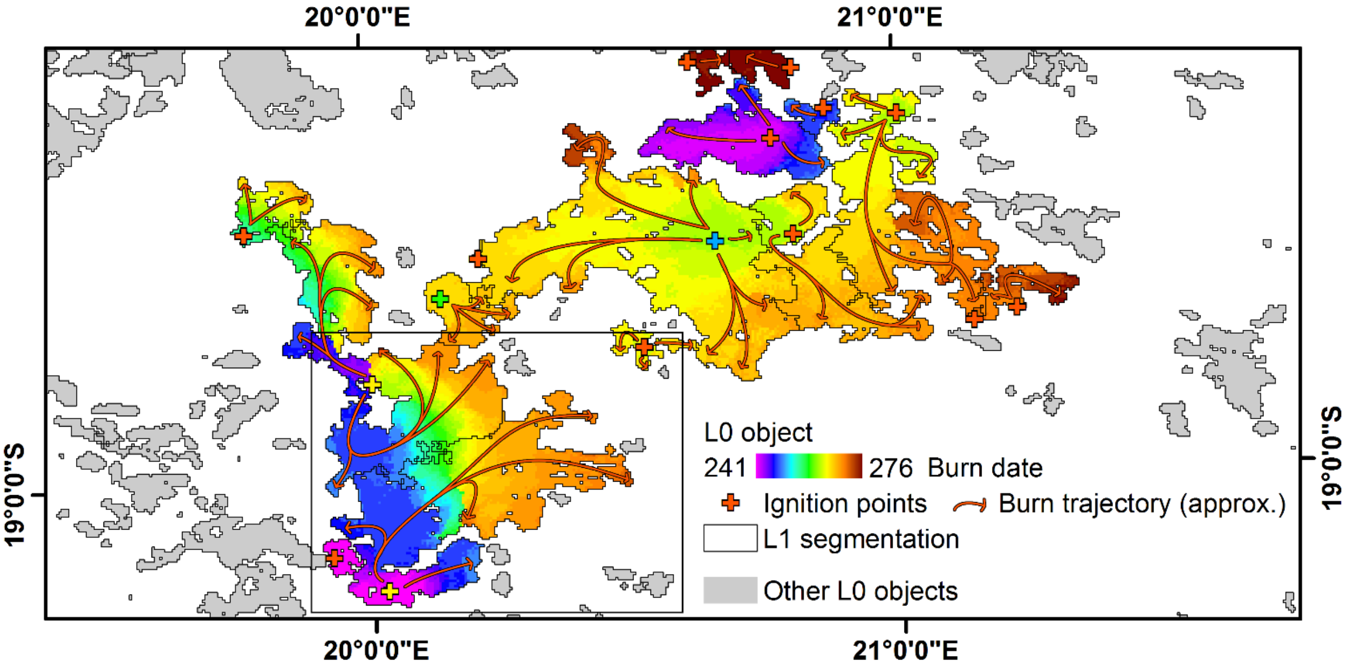

Fig. 6. Ignition points, L1-segmentation and burn dates for a large L0-fire in season 6. Other L0-fires are drawn in grey. The approximate burning trajectories are visualized with arrows that have their origin in the detected ignition points; trajectories are drawn manually for illustration purposes only. The area in the box is shown in Fig. 7.

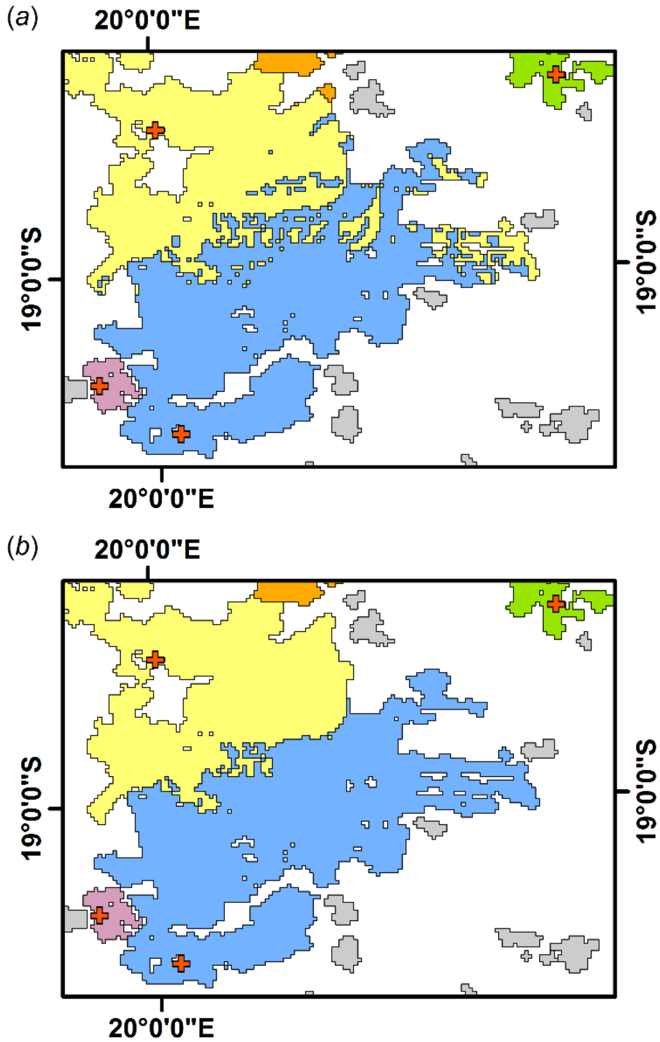

Fig. 7. Ignition points and L1-segmentation for a large L0-fire in season 6. Other L0-fires are drawn in grey. The area corresponds to the box in Fig. 6. The L1-segmentation is shown before (*a*) and after the re-assignment of non-seed patches (*b*). The colors indicate different L1-objects.

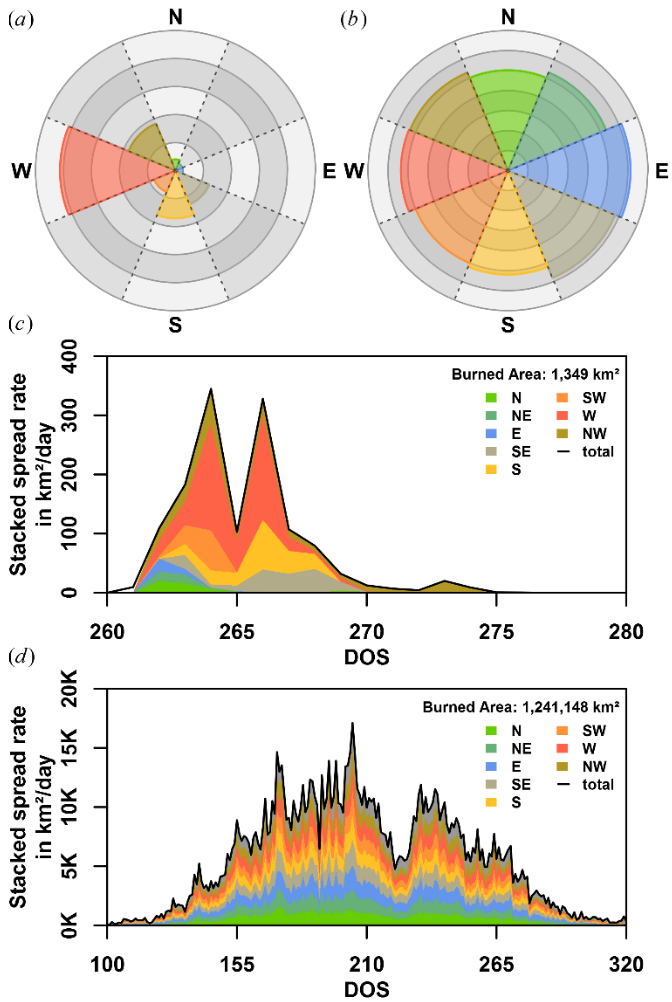

Fig. 8. (*a*): Total directional spread of a large fire in season 6 (Fig. 6, blue signature). (*b*): Total directional spread of all fires in season 6. (*c*): Stacked directional spread rates of a large fire in season 6 (Fig. 6, blue signature). (*d*): Stacked directional spread rates of all fires in season 6. The directions are computed relative to the ignition point. The specified burned area was calculated under the assumption that each pixel was completely burned. The analysis was performed in a locally adapted Lambert Azimuthal Equal Area projection, as such directional information might be distorted to a small degree.

Table 1. Summary of the tweakable algorithm parameters.

Symbol	Meaning	Unit	Default
D_s	search distance for seed aggregation	pixel	10
D_r	search distance for fire tracking	pixel	10
D_t	temporal distance for active fire detection	days	5
D_l	kernel radius for smoothing the burn dates	pixel	3
n_{min}	minimum size of burned area	pixel	2

Table 2. Number of fires, total size, average/maximum size and average/maximum lifetime of all fires in continental southern Africa per season.

Sizes are reported in km², lifetimes in days. The sizes were calculated under the assumption that each pixel was completely burned.

Season	Number of fires	Total size	Average size	Max. size	Average lifetime	Max. lifetime
1: Jan.–Dec. 2000	129,137	1,021,884.2	7.91	2237.00	5.97	108
2: Jan.–Dec. 2001	117,588	843,537.2	7.17	3527.75	4.99	92
3: Jan.–Dec. 2002	158,635	1,060,113.2	6.68	2107.50	5.93	127
4: Jan.–Dec. 2003	146,026	1,195,291.8	8.19	2046.50	6.69	147
5: Jan.–Dec. 2004	142,287	1,276,033.2	8.97	1842.00	6.96	126
6: Jan.–Dec. 2005	154,378	1,241,147.5	8.04	1666.75	6.61	131
7: Jan.–Dec. 2006	144,724	1,254,867.8	8.67	3924.75	6.81	133
8: Jan.–Dec. 2007	141,742	1,139,115	8.04	2771.25	6.40	148
9: Jan.–Dec. 2008	141,898	1,223,572.5	8.62	4572.75	6.68	132
10: Jan.–Dec. 2009	137,141	1,125,402.2	8.21	2018.75	6.52	120
11: Jan.–Dec. 2010	148,310	1,332,798.8	8.99	2443.75	6.77	165
12: Jan.–Dec. 2011	144,501	1,300,076	9	3413.25	6.62	117
13: Jan.–Dec. 2012	143,025	1,188,823.8	8.31	4409.50	6.47	126
14: Jan.–Dec. 2013	146,920	1,182,310	8.05	1882.00	6.74	146
15: Jan.–Dec. 2014	141,245	1,120,408.8	7.93	1925.25	6.57	134